HHS Public Access

Author manuscript

JCIS Open. Author manuscript; available in PMC 2023 August 17.

Published in final edited form as:

JCIS Open. 2022 October ; 7: . doi:10.1016/j.jciso.2022.100058.

The influence of calcium ions (Ca^{2+}) on the enzymatic hydrolysis of lipopolysaccharide aggregates to liberate free fatty acids (FFA) in aqueous solution

Jessika Pazol[a,b,*], **Thomas M. Weiss**[c], **Cristian D. Martínez**[b], **Orestes Quesada**[b,d], **Eduardo Nicolau**[a,b]

[a]Department of Chemistry, University of Puerto Rico, Rio Piedras Campus, 17 Ave. Universidad Ste. 1701, San Juan, PR, USA, 00925-2537

[b]Molecular Science Research Center, University of Puerto Rico, 1390 Ponce De Leon Ave, Suite 2, San Juan, PR, USA, 00931-3346

[c]Stanford Synchrotron Radiation Lightsource, SLAC National Accelerator Laboratory, Menlo Park, CA, USA, 94025

[d]Departments of Physical Sciences and Chemistry, University of Puerto Rico, Rio Piedras Campus, 17 Ave. Universidad Ste. 1701, San Juan, PR, USA, 00925-2537

Abstract

The chemical environment in aqueous solutions greatly influences the ability of amphiphilic molecules such as lipopolysaccharides (LPS) to aggregate into different structural phases in aqueous solutions. Understanding the substrate's morphology and conditions of aqueous solution that favor both enzymatic activity and the disruption of LPS aggregates are crucial in developing agents that can counteract the new trend of multidrug resistance by gram-negative bacteria. In this study, we developed two LPS morphologies using LPS from *Escherichia coli* as a model to study the *in vitro* hydrolytic response when using a lipase treatment. The hydrolysis was performed using lipase b from *Candida antarctica* to understand the catalytic effect in removing fatty acids from its lipid A moiety on different LPS aggregates. Physical and chemical characterizations of the products included dynamic light scattering, small angle X-ray scattering, Fourier transform infrared spectroscopy, thin-layer chromatography, and gas chromatography. Our results suggest a trend of prominent hydrolytic response (72% enhancement) upon the addition of calcium ions to induce LPS aggregates into bilayer formations. Moreover, our results revealed the detection of myristic acid (C14:0) as the product of the hydrolysis when using RaLPS in its aggregate forms.

*Corresponding author. Department of Chemistry, University of Puerto Rico, Rio Piedras Campus, 17 Ave. Universidad Ste. 1701, San Juan, PR, USA, 00925-2537., jessika.pazol@upr.edu (J. Pazol).

Declaration of competing interest

The authors declare that they have no known competing financial interests or personal relationships that could have appeared to influence the work reported in this paper.

Appendix A. Supplementary data

Supplementary data to this article can be found online at https://doi.org/10.1016/j.jciso.2022.100058.

Keywords

Hydrolysis; Lipopolysaccharide; Aggregate; *Candida antarctica* lipase B; Calcium

1. Introduction

Lipopolysaccharides (LPS) notably resemble amphipathic particles with a natural tendency to self-aggregate in water, which has raised interest in further exploring these interactions at the molecular level. Clinical studies have established a direct relationship between LPS aggregates and its associated toxic effects in humans [1–3]. LPS is an amphiphilic molecule comprising hydrophilic polysaccharide groups and hydrophobic acyl chains [4]. More specifically, the rough strain Ra LPS EH100 is composed of a core oligosaccharide and a lipid A moiety (Fig. 1). The initial chemistry of the aqueous media greatly affects the self-aggregation of LPS, thereby affecting its morphological structure (Fig. 1a–b) [1,4–6].

Aggregate formation of lipopolysaccharides is a complex phenomenon that depends on multiple factors such as the gram-negative bacterial strain, molecular concentration, ionic strength, and the presence of other reagents (i.e., antimicrobial peptides). Previous studies have shown that different LPS chemotypes (ranging from smooth to rough strains) diverge into various aggregate structures, particularly under various aqueous conditions [7–9]. Different LPS aggregation properties have been previously revealed using cryogenic transmission electron microscopy [7,8]. In pure water, Ra LPS has a molecular association in an organized assembly similar to elongated micellar structures [8], where the lipid moiety orients inward in the direction of the core while the head groups orient outside forming a corona. This incompatibility of the moieties in liquid phases facilitates the formation of aggregated structures. Moreover, the presence of divalent cations, such as Ca^{2+} and Mg^{2+}, plays a crucial role in the dynamics of molecular aggregation [7]. Divalent cations induce the formation of interconnected bridges via phosphate groups, which promote the formation of extended bilayer aggregates [9, 10]. Low calcium concentration in water has been shown to significantly induce the formation of stacked lamellar aggregates that promote supramolecular structures of LPS [9]. The different envisaged LPS aggregates are illustrated in Fig. 1a and b.

Establishing the hydrolytic effect of lipase treatment as a function of the aforementioned LPS aggregates remains elusive. Previous studies have used extruded LPS that has been dephosphorylated [11] and deacylated [12,13] to explore biomedical implementations. Multiple biomedical studies involve methods that either extrude molecules or include the addition of surfactants to obtain a dispersed solution. However, these pretreatment steps might interfere with the spontaneous formation of aggregates in solution, which requires elucidation from a chemical perspective. Likewise, it would be interesting to investigate the molecular interactions of different LPS aggregates using dissimilar aqueous conditions, and analyze the effect on enzymatic activity to remove the acyl chain of the lipid A moiety. This is also important because previous works have identified that even a partial removal of the lipid A free fatty acids (FFA) will significantly reduce LPS biological activity due to the lack of detection of its molecular components by the toll-like receptor TDR4 [13–16]. Likewise,

the remarkable low permeability of LPS layer towards external disruptors is part of the organisms' mechanism of protection [17] and inducing variations in this component might ease the penetration of some agents that can counteract the multidrug resistance effect. To assess this lipid content removal effect on LPS aggregates, structural variations were induced by using different water conditions (presence or absence of calcium) along with a lipase as a model.

Lipase B from *Candida antarctica* (CALB) is a versatile lipase that has been widely employed in different research studies [18–20]. It shows stable activities during thermal treatment or variation of the ionic strength [21,22]. Thereafter, the product of the reaction was characterized to confirm the expected liberation of the acyl chains (free fatty acids) and evaluate the efficacy of the hydrolytic reactions. CALB is a medium-sized enzyme belonging to lipases (EC 3.1.1.3) [23]. It is a globular α/β protein, which can hydrolyze a wide range of substrates including lipids, esters, alcohols, and acids [24]. The 33 kDa enzyme contains 317 amino acid residues as part of its primary structure [25]. It has also been applied in biodiesel production, polymer degradation, and triglyceride modification [26–31]. Lipase B has a hydrophobic pocket near the active site, which allows its absorption on hydrophobic surfaces. Once adsorbed, it can undergo cleavage at the interface and acts as an interfacial enzyme [32]. The catalytic triad of CALB is composed of Asp187, His224, and Ser105 (Asp –His–Ser) [33] as illustrated in Fig. 1c. The special arrangement of the amino acid triad forms a cavity that enables the uptake of bulky lipid substrates (e.g., triacylglycerol molecules and castor oil) [23,29,34,35].

Here, we provide comprehensive insights into both the spontaneous formation of LPS in the presence and absence of calcium and its *in vitro* hydrolysis using enzymatic reactions under different aqueous conditions. To investigate the effect of enzymatic activity on the aggregates, we used a lipase to hydrolyze the ester linkage that binds short fatty acid chains (Fig. 1c) of the lipid portion. We employed two different LPS aggregates by varying the content of divalent cations in aqueous media (0 and 10 mM Ca^{2+}) as substrates for the enzymatic reaction. Furthermore, we used a mutant LPS type (EH100 mutant Ra LPS) that includes only the core oligosaccharide fragment and lipid A moiety (Fig. 1c) [36]. To study the feasibility of this working model, we used commercially available lipase and Ra LPS as a stable formulation baseline. The Ra LPS chemotype was selected over other rough strains because it contains most sugar moieties in the core oligosaccharide region without the O-antigen portion, which would correspond to a smooth LPS chemotype. We used CALB to cleave the ester bond of the molecule. Thereafter the product of the reaction was characterized accordingly to confirm the expected liberation of the acyl chains (free fatty acids) and thus evaluate the hydrolytic reaction efficacy.

2. Materials and methods

2.1. Materials

LPS of Escherichia coli EH100 (Ra) strain was purchased from Hycult Biotech Inc. (HC4046, Uden, The Netherlands) and used without further purification. CALB, (Novozym®435) was purchased from Novozymes (Bagsvaerd, Denmark). Thin-layer chromatography (TLC) plates (20 × 20 cm) were purchased from Fisher Scientific

(Waltham, MA, USA). The solvents used (chloroform, methanol, petroleum ether, and diethyl ether) were purchased from Sigma-Aldrich (St. Louis, MO, USA) and used without further purification. High-purity silica gel (Partisil K6 60 A), phosphate buffered saline (PBS pH 7.4), Supelco FAME's C4–C2, calcium chloride ($CaCl_2$), and endotoxin-free ultrafiltered sterile water were purchased from Sigma-Aldrich (St. Louis, MO, USA).

2.2. Samples preparation

To prepare the aggregates, we used a stock solution (1 mg/mL) of LPS in ultrapure endotoxin-free double-distilled sterile water. The unextruded LPS stock solution was initially equilibrated at room temperature (from 4 °C to 20 °C) and vortexed for 10 min. For the samples containing calcium (Ca^{2+}), the concentration was adjusted to 10 mM $CaCl_2$ (from a 1 M $CaCl_2$ stock solution) before experiments.

2.3. Hydrolytic reaction

Enzymatic reactions were conducted at pH 7 using glass vials to study the release of free fatty acids from different LPS aggregates. Initially, LPS hydrolysis in pure water was conducted in a reaction mixture (500 μL) containing 150 μL of LPS stock solution (1 mg/mL), 350 μL of ultrafiltered endotoxin-free water, and 10 mg of CALB beads. Enzymatic hydrolysis of LPS in the presence of calcium ions (Ca^{2+}) were conducted by adding $CaCl_2$ at 10 mM final concentration to the reaction mixture mentioned above. The hydrolysis conditions were: 48-h reaction time, 40 °C incubation temperature, and 40 rpm speed. The reaction was stopped by removing CALB beads from the reaction mixture via physical filtration and further biophysical characterizations were conducted.

2.4. Characterization of hexa-acylated LPS (Ra) and deacylated LPS

The hydrodynamic radius and zeta potential of hexa-acylated LPS (Ra) in aqueous media were measured using a Malvern ZetaSizer Nano Series (4 mW, 632.8 nm laser). Fourier transform infrared (FTIR) spectra were recorded using a Thermo Scientific Nicolet Continuum iS50 infrared (IR) instrument coupled with a specular aperture grazing angle accessory (SAGA®). An aliquot of 200 μL LPS solution in pure water only or in the presence of calcium (1 mg/mL 10 mM $CaCl_2$) was deposited over a cleaned gold wafer <100> and allowed to air-dry overnight. Thereafter, the spectra were recorded in the reflectance mode from 400 to 4000 cm^{-1} using a 4 cm^{-1} resolution and 96 scans. A gold substrate was used to collect the background spectra. After the enzymatic reaction, the liberated fatty acid product of interest was recovered from the corresponding aqueous solution to record the infrared spectra.

2.5. Small angle x-ray scattering (SAXS)

The samples for SAXS analysis had a solution concentration of 10 mg/mL Ra LPS in 0, 10, and 100 mM $CaCl_2$. Untreated and treated Ra LPS samples were used to conduct the measurements as initially prepared in aqueous solutions without further organic extraction procedures. SAXS data were collected at beamline 4–2 [37] of the Stanford Synchrotron Radiation Light Source (SSRL), Menlo Park, CA. The sample-to-detector distance was set at 1.1 m with an X-ray wavelength of $\lambda = 1.127$ Å (11 keV). Using a Pilatus 3 × 1 M

detector (Dectris Ltd, Switzerland), the setup covered a range of momentum transfer q ≈ 0.01–0.73 $Å^{-1}$, where q is the magnitude of the scattering vector defined as $q = 4\pi \sin\theta/\lambda$, θ is the scattering angle, and λ is the wavelength of X-rays. Aliquots of 30 μL of samples were inserted into the automated sample loader at the beamline [38]. Consecutive series of 64 exposures each of 2 s were collected for the buffer blank, followed by the LPS samples. The solutions were oscillated in a stationary quartz capillary cell during data collection to maximize the exposed volume and reduce the radiation dose per exposed volume. The collected data were radially integrated, screened for the effects of radiation damage to the sample, scaled according to the transmitted beam intensity, and the corresponding values for the buffer were subtracted using an automated data reduction pipeline at the beam line.

The measured SAXS intensities for the treated and untreated LPS samples in pure water was fit using the form factor of a model core-shell particle with three concentric shells, discrete steps in electron density and an adjusted Gaussian size distribution of the core radius [39]. A background term, bkg, was allowed to account for slight inaccuracies in buffer subtraction. The electron density of the solvent (water) was set to 0.333 $Å^{-3}$ and the values reported are the electron density differences with respect to the solvent. The fitted values are summarized in the supplementary section Table S1. The reported size of the micelles includes the first two shells where the electron density is significantly larger than the solvent.

The data for the samples containing calcium (10 mM $CaCl_2$) was fit using a unilamellar vesicle form factor as detailed in Ref. [40]. The model uses gaussians electron density profile (with amplitude A, position R and width σ) to describe the inner bilayer leaflet, the outer bilayer leaflet, and the hydrocarbon trough at the center of the bilayer, respectively. It also takes into account of the influence of the overall radius of the bilayer, R0. A background term, bkg, was allowed to account for slight inaccuracies in buffer subtraction. To reduce the number of free parameters, the position of the central gaussian was fixed at 0. The fitted values are also summarized in the supplementary section Table S2. The reported size of the bilayer was determined as the peak-to-peak distance in the electron density profile.

The fitting for the two different models was done using a simulated annealing procedure followed by a nonlinear least squares fit both implemented with algorithms taken from the GSL library v2.6 [41].

2.6. Extraction and methylation of fatty acids, and subsequent isolation of fatty acid methyl esters (FAMEs)

Briefly, the lipid components of the samples were extracted according to the Folch method using 2.9×10^{-5} M butylated hydroxytoluene [42, 43]. The extracted lipids were dried under nitrogen and further dissolved in 10% methanol:diethyl ether (DE) for methylation using diazomethane (0.5 mL), as reported elsewhere [44]. The reaction was stopped by adding petroleum ether (PE) and water (2:1 v/v) after 15 min. FAMEs were separated from other lipids using rhodamine 6G-stained silica gel TLC plates developed with the PE:DE (98:2 v/v) fraction. The band corresponding to FAME was identified by comparing the retention factor (R_f) with that of a standard FAME sample simultaneously developed on the same TLC plate and visualized using a UV light source. The band was excised, extracted with

petroleum ether: diethyl ether (2:3 v/v), transferred into vials, and sealed under nitrogen for further analysis.

2.7. FAME analysis by TLC and gas chromatography (GC)

The isolated FAMEs were analyzed using an Agilent 7890 A gas chromatograph coupled to a G3431 flame ionization detector (GC-FID) with helium as the carrier gas. The GC-FID was equipped with an Agilent J&W DB-23 capillary column [(50%-cyanopropyl)-methylpolysiloxane capillary, 250 μm I.D., 0.15 μm film thickness; Agilent Santa Clara, CA, USA]. Analytes dissolved in carbon disulfide were injected in manual mode using an interfaced computer program (injector temperature 230 °C and oven temperature 150 °C). After 1 min, a 5 °C/min ramp was applied up to 220 °C (1-min hold), and the ramp was resumed to 220 °C with a 3-min hold as the final step. Peak areas were measured using ChemStation software, and peaks were identified by comparing the retention times of each peak with those obtained in a sample of FAME analytical standards (Supelco FAME's C4–C2 Lot LB98964, Sigma-Aldrich), and by graphic correlation to the values of equivalent chain lengths. FAMEs were quantified using the same FAME analytical standards.

2.8. Specific CALB hydrolytic activity with LPS

LPS hydrolysis in the presence of CALB was investigated at neutral pH. The extinction coefficient of the product of free fatty acid (FFA) hydrolysis was determined by measuring the absorbances of palmitic acid solutions with different concentrations. The activity was assayed by preparing a set of two vials (1 mL each) under different experimental conditions containing 1:20 (w/w) Ra LPS and CALB beads. Hydrolysis was conducted at 40 °C with gentle motion for 48 h. For hydrolysis in the presence of Ca^{2+}, 10 mM Ca^{2+} was used. FFA concentration was measured at 570 nm using a UV–Vis spectrophotometer Genesys 10 S VIS (Thermo Fisher Scientific, Massachusetts, USA). One unit of activity was defined as the amount of FFA produced per unit time (nmol of FFA $\cdot h^{-1}$). All assays were repeated twice at each condition.

2.9. Kinematic parameters by lineweaver-burk plot for the CALB–LPS system

The kinetic parameters K_m and V_{max} were determined using the Lineweaver–Burk plot constructed using Origin Graphing and Analyzing software version 95 E (Northampton, MA, USA). Ra LPS (EH100) at different concentrations was used as substrate for deacylation reaction. Samples were hydrolyzed for 48 h at 40 °C. After completion of the reaction, the liberated fatty acid content was determined by thermometric titration using a standardized KOH solution, where the temperature against titrant volume was recorded using a thermoelectric thermometer. Equivalent moles of acid were divided by the reaction time and weight of the immobilized enzyme under both solution conditions. Experiments were performed in triplicate (n = 3), and data are presented as the average with standard deviation (±SD).

3. Results and discussion

To investigate the hydrolytic response of LPS via enzymatic hydrolysis using CALB, micellar LPS aggregates were initially obtained in aqueous media using pure water. Ca^{2+}

(10 mM) was then added to change the solution conditions and the aggregate forms of LPS. The structures were characterized and described in the section containing small-angle X-ray scattering results. The released FFAs were extracted and used to determine the effect of lipase. The untreated and treated samples (before and after hydrolysis, respectively) were physically and chemically characterized to assess the lipase activity over different LPS morphologies. For clarification purpose, all figures were color-coded and/or pattern-coded to indicate different sample conditions. In general, the black figures correspond to LPS solution in pure water (LPS-0), whereas the red figures correspond to aqueous LPS solution containing 10 mM $CaCl_2$ (LPS-10).

3.1. Dynamic light scattering (DLS) measurement

The size of self-aggregated LPS was measured prior the hydrolysis using DLS. Hydrodynamic diameter (D_H) values (Fig. 2) confirmed the size difference between the two initially untreated LPS structures. The D_H of LPS in pure water was 105.7 ± 0.6 nm. On the other hand, LPS solution with Ca^{2+} (Fig. 2b) showed a relatively larger hydrodynamic diameter of 1106.4 ± 1.3 nm.

Thereafter, measurement of the zeta potential (ζ) indicated a highly negative surface charge of LPS aggregates in pure water (−50.7 ± 0.6 mV, Fig. 2c) for the conditions used in LPS-0 sample. Subsequently, a nearly neutral zeta potential was observed for the LPS-10 sample containing calcium ions (−9.1 ± 0.7 mV, Fig. 2d).

These results confirmed the key role of divalent cations in the aqueous conditions, where calcium ions (Ca^{2+}) specifically interacted with the negatively charged surface of the molecule. Positive divalent ions influence the formation of interconnected bridges with phosphate groups on LPS, therefore, promoting the formation of extended bilayer aggregates [9].

3.2. SAXS analysis

Synchrotron-based SAXS was used to probe and analyze the nanostructures of the different LPS aggregates. We aimed to corroborate the differences in the structures for all untreated and treated samples. To achieve this aim, we prepared two different LPS solutions: one in nanofiltered water (18.2 MΩ-cm^2, LPS-0), and a second in water containing 10 mM $CaCl_2$ (LPS-10). The obtained SAXS profiles are shown in Fig. 3. A third additional LPS sample at a higher calcium concentration 100 mM $CaCl_2$ was also included as part of the supplementary information section (Figure S3). The method for the samples preparation and fitting model are detailed in section 2.5 (Small angle x-ray scattering).

The scattering profiles of log I(q) versus log(q) are shown in Fig. 3 for the LPS-0 and LPS-10 samples. The intensities of the untreated samples are illustrated in a void-dot pattern, whereas the solid dot patterns indicate the data for the treated samples.

The SAXS profiles provides information on the overall shape and size of the self-assembled LPS particles. Initially, we compared the profiles with previous related LPS SAXS results (Fig. 3) reported earlier in the literature [7,8]. Indeed, LPS nanostructures have complex morphologies that change upon varying the saccharide groups as well as the aqueous media

content. Our results for LPS-0 samples (Fig. 3a) are concurrent with previous reported SAXS profiles of LPS containing long saccharide groups, also known as rough chemotype, Ra LPS and Re LPS [7,45].

Moreover, the SAXS profiles were further analyzed using a fitting micellar model with multiple concentric shells [39] for the LPS-0 samples and a vesicular bilayer model [40] for LPS-10 samples. The multiple shells in the model are necessary to adequately describe the gradual decay of the electron density within the discrete model (Fig. 3a inset). The main structural features of the LPS nanostructures extracted from the fitted parameters are summarized in Table 1. The complete set of fit parameters are tabulated in tables S1 and S2 located in the supplementary information.

The fit analysis to the SAXS profiles revealed that the untreated samples had initially dissimilar LPS morphologies: micelle (LPS-0) and bilayer structure (LPS-10). The bilayer formation is associated with the addition of divalent cations such as Ca^{2+} that induces the formation of calcium bridges and interconnects LPS molecules via phosphate groups [6,9,10]. This confirms the initial structural differences of LPS samples before conducting the enzymatic treatment.

After completing the enzymatic treatment, the samples fitting models were also verified. In spite there are visible differences in the scattering profiles for the LPS-0 samples (untreated and treated), the micellar fitting model revealed only a subtle size reduction from 58.5 ± 4.0 Å to 55.9 ± 4.0 Å. For the bilayer model, the fitting analysis also resulted in a slight change of the corresponding d_b distance (Fig. 3b inset) from 55.2 ± 1.1 Å to 54.4 ± 1.1 Å. These fitting results indicate that despite affecting the chemical composition by removing lipid content from the molecule using the lipase, the biophysical properties of size and shape did not show large differences. However, the fitting model analysis revealed that when the solution contained calcium (LPS-10), a sharpening of the outer leaflet for the bilayer structure is observed after the enzymatic treatment (Fig. 3b, inset for electron density curves). In addition, the width distance σ for the outer bilayer leaflet decreased from 8.2 ± 0.1 Å to 6.2 ± 0.1 Å (Table 1), thus revealing less disorder in its structure.

The observed results are interesting because the fitting model for the SAXS profiles not only reveals the initial differences in LPS nanostructures, but also suggest that the combination of calcium and enzymatic treatment improves the overall symmetry of the bilayer structure using the LPS-10 sample conditions. Please refer to a complete summary of the fitting parameters in the supplementary information section (Table S1).

3.3. FTIR spectra of Ra-LPS

The functional groups of the LPS samples (before and after the enzymatic treatment) were characterized by FTIR spectroscopy using the grazing incidence reflectance mode. FTIR instrument was coupled with SAGA® accessory to intensify the signals for the functional groups of interest. All samples were subjected to the extraction and methylation procedure described in the method section 2.6. The extraction and purification of the samples were necessary because the intensities of the bands were weak in aqueous media.

In general, the spectra (Fig. 4) of the initial LPS-0 and LPS-10 samples were collected to assess any difference within the infrared region (400–4000 cm^{-1}) before conducting the hydrolysis. The spectra of the untreated LPS samples revealed three characteristic bands for the functional groups associated with the molecule (Fig. 4 dotted lines). The two consecutive bands at 2924 and 2958 cm^{-1} (C–H symmetric stretch) and the band near 1462 cm^{-1} (CH_2 bend) indicate the presence of aliphatic carbon chains associated with FFAs [46]. Therefore, similar functional groups were observed in both initial spectra (LPS-0 and LPS-10).

Thereafter, we obtained the infrared spectra to verify the expected functional groups after the hydrolysis (Fig. 4 solid line). The anticipated signals should correspond to that of a carboxylic functional group associated to the free fatty acid (FFA) product formation after conducting the hydrolytic reaction. The liberated fatty acids after the enzymatic reaction confirms the effect of the lipase at different aggregates conditions. The bands of interest were highlighted at the following wavenumbers: 1178 cm^{-1} (C–O–C stretch), 1358 cm^{-1} (O–H bend), and 1725 cm^{-1} (C═O stretch) and are associated to bonded ester carboxylic carbons [47]. The signals for the two consecutive bands at 2924 and 2958 cm^{-1} (C–H symmetric stretch) significantly decreased in both samples after the hydrolysis. Methylation of the liberated FFAs can be related to this intensity reduction near 2829 cm^{-1} ($C–CH_3$ stretch) since the molecular composition is change after the enzymatic reaction [47]. Notably, both treated samples conditions (LPS-0 and LPS-10) revealed the effect of the hydrolysis on the aggregates when using the lipase model. This was confirm with the expected signals of the carboxylic ester functional group of the liberated fatty acids chains.

3.4. TLC and GC-FID analysis

The lipid product was extracted and converted into FAME as previously described [44]. The lipid mixture was separated using a fluorescent silica gel TLC plate as shown in Fig. 5.

The lipid products were extracted and converted to FAME as previously described [43]. As shown in Fig. 5, separation of the lipid portion from the sample was achieved using a fluorescence silica gel TLC plate developed with PE:DE (98:2 v/v).

Thereafter, we identified a band aligned with the standard spot of FAME (C4–C24) that interfered with the fluorescence signal (Fig. 5). The band had R_f values of 0.18 (LPS in pure water) and 0.29 (LPS in 10 mM Ca^{2+}). The LPS sample containing Ca^{2+} was run on a different TLC plate on a different day, and therefore, showed a different R_f value. Nevertheless, sample migration was also corroborated against a FAME standard that was run on the same TLC plate. Differences in R_f values in the developed TLC plates might be associated with different factors, such as adsorbent thickness, the exact composition of the mobile phase, temperature, and wetting of the plate. The R_f values confirmed the effectiveness of solvent separation for the lipid mixture, which contained at least three components in both samples. Qualitative assessment revealed that the sample containing 10 mM Ca^{2+} showed a relatively strong fluorescence spot interference signal in all TLC plates. Moreover, fewer migrating breakdowns of components were observed in this sample. More importantly, both TLC plates under the two different conditions confirmed the presence of liberated fatty acids, thereby confirming the breakdown of LPS aggregates with different morphologies.

Subsequently, the FAME band was isolated for GC-FID analysis. To identify the corresponding peaks for the sample treated in pure water, the retrieved retention times were compared to the chromatogram of a standard FAME (C4–C24) mix (see supplementary document Figure S5). The chromatogram of the extracted sample revealed two peaks at the retention times of 4.47 min and 13.36 min. The first identified peak at 4.47 min corresponded to the saturated fatty acid product of methyl myristate (C14:0). Although the second peak (13.36 min) appeared after the tricosanoic acid (C23:0) signal (13.0 min), it did not match any of the remaining peaks in the chromatogram of the FAME standard. Afterwards, the amount of liberated fatty acid was calculated with respect to an external FAME standard mixture and using the equation for calibration factor as previously described [48]. FAME was quantified using the following equation:

$$C_F = \frac{A_S}{C_S} \tag{1}$$

where C_F is the calibration factor, A_S is the peak area of the standard, and C_S is the standard concentration. The average CF was then used to calculate the sample concentration (C_{FA}) using the sample area peak (A_{FA}) with the following formula:

$$C_{FA} = \frac{A_{FA}}{CF} \tag{2}$$

The concentration and sample volume were used to estimate the fatty acid content of the sample in pure water. The results are reported in micrograms of fatty acid (C14:0) per milligram of initial LPS content. Myristic acid was found to be the only fatty acid product with a concentration of 0.01455 μg/mg. The other bands on the TLC plates were also analyzed by GC-FID, but the results did not reveal any corresponding fatty acid signals in the chromatogram. Notably, in accordance with the results of the chromatogram, only partial hydrolysis occurred instead of complete removal of the acyl chains of LPS.

The aim of this study was to probe the effect of enzymatic activity on two distinct LPS morphologies. The results of GC-FID analysis indicated partial hydrolysis of LPS aggregates using CALB. CALB can cleave the secondary acyl chain (C14:0) from lipid A moiety under both aqueous conditions. The lipid A moiety of the Ra LPS includes four primary acyl chains attached to the diglucosamine backbone and two secondary acyl chains linked to the primary ones. Presumably, the hydrophobic pocket of the enzyme may approach and cleave the secondary acyl chain connected to the remaining moieties of LPS, as indicated by the number of carbons in the acyl chain identified by the GC assay. This result is in agreement with previous studies that used CALB as a carboxylic ester hydrolase with substrates other than LPS [49].

3.5. Lineweaver-burk plot

The rate of product formation (FFA) was investigated to further characterize the hydrolytic reaction. Since CALB can catalyze a broad spectrum of substrates [32,49], we studied the kinetics of the different LPS structures that remained elusive. The kinetic parameters were best fitted using the Michaelis–Menten [50] equation and the Lineweaver–Burk plot [51]

(Fig. 6) at sub-milligram amounts of the substrate. In the latter method, the rate of product formation (using a fixed amount of enzyme) satisfies the following equation:

$$\upsilon = \frac{1}{\upsilon_{max}} + \frac{K_M}{\upsilon_{max}} \cdot \frac{1}{[S]} \quad (3)$$

where υ is the velocity of product formation, K_M is the Michaelis–Menten constant, and [S] corresponds to substrate concentration. K_M estimation in the kinetic model facilitates the assessment of affinity between the active site of an enzyme and biological substrate [51].

The resulting parameters (Table 2) show that CALB interacted with both the aggregated morphologies of LPS. For the CALB–LPS system, the observed K_m was 28.6 μM for LPS in nano pure water and 84.2 μM for LPS with Ca^{2+}. V_{max} for both of these conditions were 1.41×10^3 and 2.71×10^3 μmol min^{-1} per gm CALB bead, respectively.

The obtained results confirmed a higher reaction yield after Ca^{2+} addition of to the solution. The V_{max} increased during the reaction containing 10 mM Ca^{2+}, suggesting that fatty acid chains were removed faster in the presence of Ca^{2+} ions in solution.

Furthermore, the Michaelis parameter K_m considerably increased, suggesting high LPS concentrations associated with half of the total enzyme molecules present in the reaction mixture. Therefore, a higher LPS concentration is required to reach V_{max} in presence of Ca^{2+} than in pure water only. For this enzyme/substrate pair, sub-milligram concentrations of LPS achieved the maximum catalytic effect.

3.6. Specific CALB activity in LPS hydrolysis

A colorimetric method was used to quantify the FFA content produced by the reaction, thereby mitigating the possible risk of product loss during sample handling using the TLC/GC method. Enzymatic hydrolysis was conducted near pH 7, as it favors CALB activity [52], with an incubation temperature of 40 °C. From the calibration curve, we obtained the molar extinction coefficient of palmitic acid as 5.65×10^{-11} M^{-1} cm^{-1}, R^2:0.9945 (Support information Figure S9). As shown in Fig. 7, the specific activity of the enzyme significantly increased in samples with added Ca^{2+}; the values were 0.7 ± 0.01 U/mg CALB (LPS-0) and 1.5 ± 0.1 U/mg CALB (LPS-10). The sample containing Ca^{2+} produced 72% more FFAs than did LPS in pure water, after hydrolysis.

An increased FFA content in the presence of Ca^{2+} can be explained by the fact that an interconnected sheet-like structure contains more LPS molecules than an elongated fibrillar structure; therefore, the enzyme can cleave more acyl chains. We demonstrated that CALB can remove fatty acids from LPS molecules with various architectures in different aqueous environments. We revealed that fatty acid liberation was enhanced by Ca^{2+}. Although LPS forms complex molecular structures, partial hydrolysis can be achieved to remove secondary acyl chains (C14:0) from the lipid A moiety. The presence of sugar groups in the core oligosaccharide region of Ra LPS chemotypes provides an external hydrophilic layer that might interfere with the permeabilization of antibiotics, particularly hydrophobic groups [53]. In this context, the intrinsic mechanism of the catalytic action of lipases, such as CALB, involves enzyme adsorption to the hydrophobic substrate region and therefore, acts

at the molecular interface [32]. In this study, CALB served as a model to investigate the hydrophobic interactions between different LPS aggregates and the enzyme. The hydrophobic pocket of the active site of CALB is covered by a lid made of a polypeptide chain that contains a hydrophilic external face [52]. This enzyme structure facilitates access to the hydrophilic layer of LPS aggregates formed by sugar groups. The findings of this study suggest that interfacial enzymes, such as lipases (e.g., CALB), may play a role in designing new agents that can interact with different LPS aggregates and help to counteract the new trend of multi-drug resistance by gram-negative bacteria.

4. Conclusions

In this work, we aimed to understand the hydrolytic effect on different LPS aggregate structures induced by the addition of calcium ions in the aqueous media. Our results indicate that in absence of calcium ions, Ra LPS has a micellar structure while a bilayer formation occurs upon the addition of divalent cations. Moreover, the *in vitro* enzymatic treatment using CALB partially removes the secondary acyl chain (C14:0) from the aggregates' lipid A moiety. Furthermore, small angle X-ray scattering revealed the differences in the initial LPS aggregate structures after the addition of calcium ions to the solution. Consequently, it was also observed that the treated samples (LPS-0 and LPS-10) conserved its initial shape or size after partially removing the lipid content from the aggregates. Interestingly, the distribution of the electron densities of the treated LPS-10 bilayer sample revealed an improvement for the overall bilayer symmetry. Our results suggest that the combination of calcium and enzymatic treatment of Ra LPS aggregates might be further explored as a pre-treatment step in combination with other counteracting agents' application. Despite multiple factors for multidrug resistance agents' efficacy remains complex, it is recognized that improving the bilayer symmetry along with a reduction of lipid content, may enhance the conditions to potential pore former molecules that can eventually help in the permeability of counteracting agents. Lastly, the addition of calcium ions induces a more favorable LPS structure that improves the enzymatic treatment to remove the lipids by 72%.

Supplementary Material

Refer to Web version on PubMed Central for supplementary material.

Acknowledgements

The Stanford Synchrotron Radiation Lightsource, SLAC National Accelerator Laboratory, is supported by the U.S. Department of Energy, Office of Science, and Office of Basic Energy Sciences under Contract No. DE-AC02-76SF00515. The SSRL Structural Molecular Biology Program is supported by the DOE Office of Biological and Environmental Research and by the National Institutes of Health (NIH), National Institute of General Medical Sciences (NIGMS) (including P41GM103393). The contents of this publication are solely the responsibility of the authors and do not necessarily represent the official views of the NIGMS or NIH.

The Pilatus detector at beamline 4–2 at SSRL was funded by the National Institutes of Health Grant S10OD021512.

The authors are also grateful to the UPR Molecular Science Research Center for access to resources and instruments. The authors also thank Ms. Liz de Jesus-Hernandez and Ms. Yanizbeth Yambo-Chevere for literature review. Special thanks to Dr. Robert S. Munford, senior clinician chief at the AHDS–NIH, for his valuable and helpful insights and discussion regarding the interaction of lipopolysaccharides with animal's immune system. Special thanks to Ms. Laura Penabad for her valuable help in revising the manuscript for language and grammatical errors.

Funding

This work was supported by the Research Initiative for Scientific Enhancement (RISE) Program [grant number 5R25GM061151-19] and the NASA MIRO-Puerto Rico Space Partnership for Research, Education, and Training (PR-SPRInT) [grant number 80NSSC19M0236].

References

[1]. Munford RS, Sensing gram-negative bacterial lipopolysaccharides: a human disease determinant? Infect. Immun. 76 (2008) 454–465. [PubMed: 18086818]

[2]. Gutsmann T, Schromm AB, Brandenburg K, The physicochemistry of endotoxins in relation to bioactivity, International journal of medical microbiology 297 (2007) 341–352. [PubMed: 17452014]

[3]. Weinbaum G, Kadis S, Ajl SJ, Bacterial Endotoxins: A Comprehensive Treatise, Elsevier Science, 2016.

[4]. Raetz CR, Biochemistry of endotoxins, Annu. Rev. Biochem. 59 (1990) 129–170. [PubMed: 1695830]

[5]. Sasaki H, White SH, Aggregation behavior of an ultra-pure lipopolysaccharide that stimulates TLR-4 receptors, Biophys. J. 95 (2008) 986–993. [PubMed: 18375521]

[6]. Parikh SJ, Chorover J, ATR-FTIR study of lipopolysaccharides at mineral surfaces, Colloids Surf. B Biointerfaces 62 (2008) 188–198. [PubMed: 18006288]

[7]. Richter W, Vogel V, Howe J, Steiniger F, Brauser A, Koch MH, Roessle M, Gutsmann T, Garidel P, Mäntele W, Morphology, size distribution, and aggregate structure of lipopolysaccharide and lipid A dispersions from enterobacterial origin, Innate Immun. 17 (2011) 427–438. [PubMed: 20682588]

[8]. Bello G, Eriksson J, Terry A, Edwards K, Lawrence MJ, Barlow D, Harvey RD, Characterization of the aggregates formed by various bacterial lipopolysaccharides in solution and upon interaction with antimicrobial peptides, Langmuir 31 (2015) 741–751. [PubMed: 25514503]

[9]. Redeker C, Briscoe WH, Interactions between mutant bacterial lipopolysaccharide (LPS-Ra) surface layers: surface vesicles, membrane fusion, and effect of Ca2+ and temperature, Langmuir 35 (2019) 15739–15750. [PubMed: 31604373]

[10]. Rodriguez-Loureiro I, Latza VM, Fragneto G, Schneck E, Conformation of single and interacting lipopolysaccharide surfaces bearing O-side chains, Biophys. J. 114 (2018) 1624–1635. [PubMed: 29642032]

[11]. Buts J-P, Dekeyser N, Stilmant C, Delem E, Smets F, Sokal E, Saccharomyces boulardii produces in rat small intestine a novel protein phosphatase that inhibits Escherichia coli endotoxin by dephosphorylation, Pediatr. Res. 60 (2006) 24–29. [PubMed: 16690953]

[12]. Shao B, Lu M, Katz SC, Varley AW, Hardwick J, Rogers TE, Ojogun N, Rockey DC, DeMatteo RP, Munford RS, A host lipase detoxifies bacterial lipopolysaccharides in the liver and spleen, J. Biol. Chem. 282 (2007) 13726–13735. [PubMed: 17322564]

[13]. Gorelik A, Illes K, Nagar B, Crystal structure of the mammalian lipopolysaccharide detoxifier, Proc. Natl. Acad. Sci. USA 115 (2018) E896–E905. [PubMed: 29343645]

[14]. Rietschel ET, Brade H, Holst O, Brade L, Müller-Loennies S, Mamat U, Zähringer U, Beckmann F, Seydel U, Brandenburg K, Bacterial Endotoxin: Chemical Constitution, Biological Recognition, Host Response, and Immunological Detoxification, Pathology of septic shock, 1996, pp. 39–81.

[15]. Lorenz E, Mira JP, Frees KL, Schwartz DA, Relevance of mutations in the TLR4 receptor in patients with gram-negative septic shock, Arch. Intern. Med. 162 (2002) 1028–1032. [PubMed: 11996613]

[16]. Beutler B, Rietschel ET, Innate immune sensing and its roots: the story of endotoxin, Nat. Rev. Immunol. 3 (2003) 169–176. [PubMed: 12563300]

[17]. Paracini N, Schneck E, Imberty A, Micciulla S, Lipopolysaccharides at the interface, Adv. Colloid Interface Sci. (2022), 102603. [PubMed: 35093846]

[18]. Martins AB, Graebin NG, Lorenzoni AS, Fernandez-Lafuente R, Ayub MA, Rodrigues RC, Rapid and high yields of synthesis of butyl acetate catalyzed by Novozym 435: reaction optimization by response surface methodology, Process Biochem. 46 (2011) 2311–2316.

[19]. Woudenberg-van Oosterom M, van Rantwijk F, Sheldon RA, Regioselective acylation of disaccharides in tert-butyl alcohol catalyzed by Candida Antarctica lipase, Biotechnol. Bioeng. 49 (1996) 328–333. [PubMed: 18623584]

[20]. Wang C, Wang N, Liu X, Wan P, He X, Shang Y, Expanding application of immobilized candida Antarctica lipase B: a green enzyme catalyst for Knoevenagel condensation reaction, Fibers Polym. 19 (2018) 1611–1617.

[21]. van Rantwijk F, Secundo F, Sheldon RA, Structure and activity of Candida Antarctica lipase B in ionic liquids, Green Chem. 8 (2006) 282–286.

[22]. Zhang N, Suen WC, Windsor W, Xiao L, Madison V, Zaks A, Improving tolerance of Candida Antarctica lipase B towards irreversible thermal inactivation through directed evolution, Protein Eng. 16 (2003) 599–605. [PubMed: 12968077]

[23]. Uppenberg J, Hansen MT, Patkar S, Jones TA, The sequence, crystal structure determination and refinement of two crystal forms of lipase B from Candida Antarctica, Structure 2 (1994) 293–308. [PubMed: 8087556]

[24]. Datta S, Christena LR, Rajaram YRS, Enzyme immobilization: an overview on techniques and support materials, 3 Biotech 3 (2013) 1–9.

[25]. Nicoletti G, Cipolatti EP, Valerio A, Carbonera NG, Soares NS, Theilacker E, Ninow JL, de Oliveira D, Evaluation of different methods for immobilization of Candida Antarctica lipase B (CalB lipase) in polyurethane foam and its application in the production of geranyl propionate, Bioproc. Biosyst. Eng. 38 (2015) 1739–1748.

[26]. Pellis A, Comerford JW, Weinberger S, Guebitz GM, Clark JH, Farmer TJ, Enzymatic synthesis of lignin derivable pyridine based polyesters for the substitution of petroleum derived plastics, Nat. Commun. 10 (2019) 1762. [PubMed: 30992443]

[27]. Wcisłek A, Sonseca Olalla A, McClain A, Piegat A, Sobolewski P, Puskas J, El Fray M, Enzymatic degradation of poly (butylene succinate) copolyesters synthesized with the use of candida Antarctica lipase b, Polymers 10 (2018) 688. [PubMed: 30966722]

[28]. Yadav MG, Kavadia MR, Vadgama RN, Odaneth AA, Lali AM, Production of 6-O-l-Ascorbyl palmitate by immobilized Candida Antarctica lipase B, Appl. Biochem. Biotechnol. 184 (2018) 1168–1186. [PubMed: 28971362]

[29]. Köse Ö, Tüter M, Aksoy HA, Immobilized Candida Antarctica lipase-catalyzed alcoholysis of cotton seed oil in a solvent-free medium, Bioresour. Technol. 83 (2002) 125–129. [PubMed: 12056487]

[30]. Shimada Y, Watanabe Y, Samukawa T, Sugihara A, Noda H, Fukuda H, Tominaga Y, Conversion of vegetable oil to biodiesel using immobilized Candida Antarctica lipase, J. Am. Oil Chem. Soc. 76 (1999) 789–793.

[31]. Graebin NG, Martins AB, Lorenzoni AS, Garcia-Galan C, Fernandez-Lafuente R, Ayub MA, Rodrigues RC, Immobilization of lipase B from Candida Antarctica on porous styrene–divinylbenzene beads improves butyl acetate synthesis, Biotechnol. Prog. 28 (2012) 406–412. [PubMed: 22271615]

[32]. Ortiz C, Ferreira ML, Barbosa O, dos Santos JC, Rodrigues RC, Berenguer-Murcia Á, Briand LE, Fernandez-Lafuente R, Novozym 435: the “perfect” lipase immobilized biocatalyst? Catal. Sci. Technol. 9 (2019) 2380–2420.

[33]. Stauch B, Fisher SJ, Cianci M, Open and closed states of Candida Antarctica lipase B: protonation and the mechanism of interfacial activation, J. Lipid Res. 56 (2015) 2348–2358. [PubMed: 26447231]

[34]. Juhl PB, Doderer K, Hollmann F, Thum O, Pleiss J, Engineering of Candida Antarctica lipase B for hydrolysis of bulky carboxylic acid esters, J. Biotechnol. 150 (2010) 474–480. [PubMed: 20887757]

[35]. Pazol J, Vazquez A, Nicolau E, Characterization of non-covalent immobilized Candida antartica lipase b over PS-b-P4VP as a model bio-reactive porous interface, Colloids Surf. B Biointerfaces 183 (2019), 110418. [PubMed: 31404792]

[36]. Inagaki M, Kawaura T, Wakashima H, Kato M, Nishikawa S, Kashimura N, Different contributions of the outer and inner R-core residues of lipopolysaccharide to the recognition by spike H and G proteins of bacteriophage φX174, FEMS Microbiol. Lett. 226 (2003) 221–227. [PubMed: 14553915]

[37]. Smolsky IL, Liu P, Niebuhr M, Ito K, Weiss TM, Tsuruta H, Biological small-angle X-ray scattering facility at the Stanford Synchrotron radiation laboratory, Applied Crystallography 40 (2007) s453–s458.

[38]. Martel A, Liu P, Weiss TM, Niebuhr M, Tsuruta H, An integrated high-throughput data acquisition system for biological solution X-ray scattering studies, J. Synchrotron Radiat. 19 (2012) 431–434. [PubMed: 22514181]

[39]. Pedersen JS, Analysis of small-angle scattering data from colloids and polymer solutions: modeling and least-squares fitting, Adv. Colloid Interface Sci. 70 (1997) 171–210.

[40]. Brzustowicz MR, Brunger AT, X-ray scattering from unilamellar lipid vesicles, J. Appl. Crystallogr. 38 (2005) 126–131.

[41]. Galassi M, Davies J, Theiler J, Gough B, Jungman G, Alken P, Booth M, Rossi F, Ulerich R, GNU Scientific Library, Network Theory Limited, 2002.

[42]. Folch J, Lees M, Stanley GS, A simple method for the isolation and purification of total lipides from animal tissues, J. Biol. Chem. 226 (1957) 497–509. [PubMed: 13428781]

[43]. Quesada O, González-Freire C, Ferrer MC, Colón-Sáez JO, Fernández-García E, Mercado J, Dávila A, Morales R, Lasalde-Dominicci JA, Uncovering the lipidic basis for the preparation of functional nicotinic acetylcholine receptor detergent complexes for structural studies, Sci. Rep. 6 (2016) 1–12. [PubMed: 28442746]

[44]. Quesada O, González-Freire C, Ferrer MC, Colón-Sáez JO, Fernández-García E, Mercado J, Dávila A, Morales R, Lasalde-Dominicci JA, Uncovering the lipidic basis for the preparation of functional nicotinic acetylcholine receptor detergent complexes for structural studies, Sci. Rep. 6 (2016) 32766. [PubMed: 27641515]

[45]. Garidel P, Rappolt M, Schromm AB, Howe J, Lohner K, Andrä J, Koch MH, Brandenburg K, Divalent cations affect chain mobility and aggregate structure of lipopolysaccharide from Salmonella Minnesota reflected in a decrease of its biological activity, Biochim. Biophys. Acta, Biomembr. 1715 (2005) 122–131.

[46]. Olins AL, Warner RC, Physicochemical studies on a lipopolysaccharide from the cell wall of Azotobacter vinelandii, J. Biol. Chem. 242 (1967) 4994–5001. [PubMed: 4964628]

[47]. Smith BC, Infrared Spectral Interpretation: a Systematic Approach, CRC press, 1998.

[48]. Patnaik P, Handbook of Environmental Analysis: Chemical Pollutants in Air, Water, Soil, and Solid Wastes, Crc Press, 2017.

[49]. Galmés MA, García-Junceda E, Świderek K, Moliner V, Exploring the origin of amidase substrate promiscuity in CALB by a computational approach, ACS Catal. 10 (2019) 1938–1946.

[50]. Johnson KA, Goody RS, The original Michaelis constant: translation of the 1913 Michaelis–Menten paper, Biochemistry 50 (2011) 8264–8269. [PubMed: 21888353]

[51]. Berg JM, Tymoczko JL, Stryer L, Biochemistry: International Version, Granite Hill Publishers, 2002.

[52]. Martinelle M, Holmquist M, Hult K, On the interfacial activation of Candida Antarctica lipase A and B as compared with Humicola lanuginosa lipase, Biochim. Biophys. Acta Lipids Lipid. Metabol 1258 (1995) 272–276.

[53]. Nikaido H, Molecular basis of bacterial outer membrane permeability revisited, Microbiol. Mol. Biol. Rev. 67 (2003) 593–656. [PubMed: 14665678]

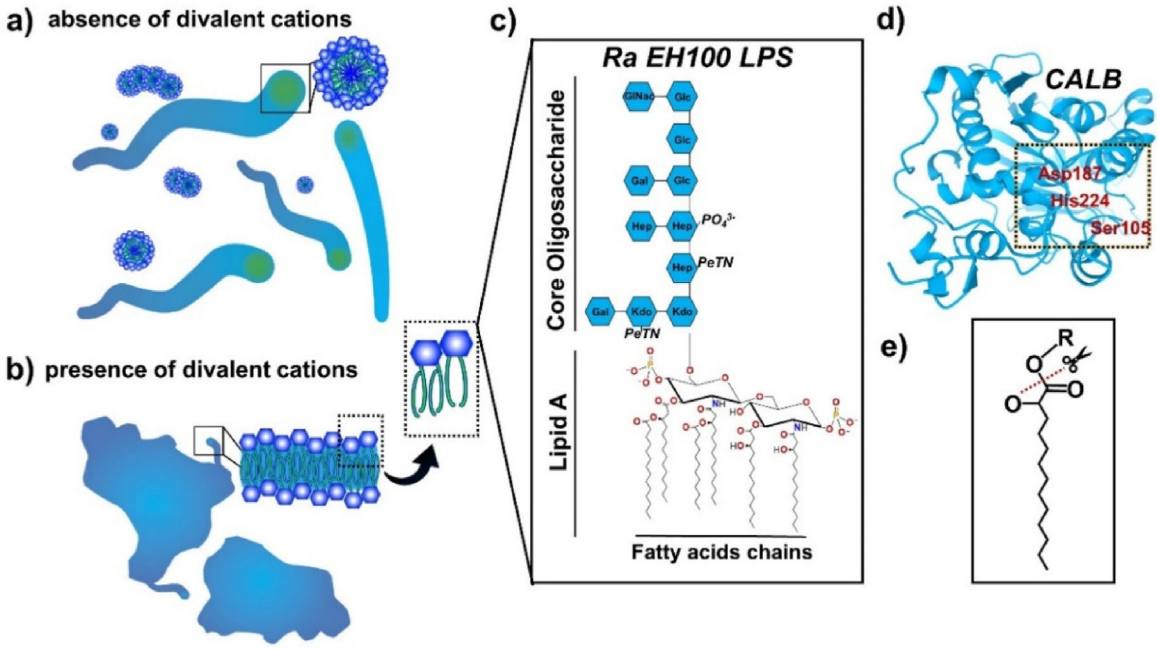

Fig. 1.

Schematics of different lipopolysaccharide (LPS) aggregates in an aqueous media, their chemical constituents, and lipase structure. (a) LPS aggregates depicting an elongated micellar form in absence of divalent cations [7]. (b) LPS aggregates forming sheet-like bilayers in presence of divalent cations [8]. (c) Chemical constitution of hexa-acylated rough LPS chemotype Ra EH100 [8] showing fatty acids in lipid A moiety with sugar groups (Kdo, 3-deoxy-D-manno-octulosonic acid; Gal, D-galactose; Hep, L-*glycero*-D-manno-heptose; Glc, D-glucose; GlNac, N-acetyl-D-glucosamine; PeTN, phosphatidyl-ethanolamine). d) *Candida antarctica* lipase B (CALB) ribbon structure retrieved from Protein Data Bank 1TCA showing its catalytic triad amino acids (Asp187, His224, and Ser105). (e) Schematic representation of the carboxylic ester bond cleaving site at lipid A moiety; the fatty acid chain is released after the hydrolytic reaction.

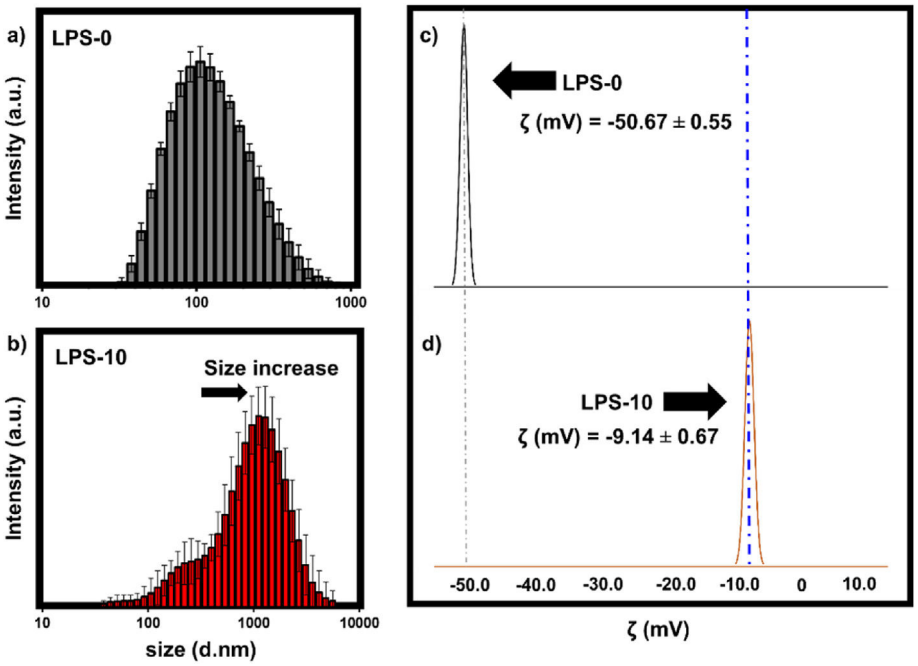

Fig. 2.

Dynamic light scattering (DLS) results at the left panel showing the measured hydrodynamic diameter of LPS (Ra EH100) aggregates, before hydrolysis, in a) pure water (LPS-0) and b) water with 10 mM Ca^{2+}(LPS-10). Zeta potential (ζ), at the right panel, of lipopolysaccharide solutions in c) pure water and d) water with 10 mM Ca^{2+} at 20 °C before hydrolysis. Data indicate the mean ± SD, n = 3.

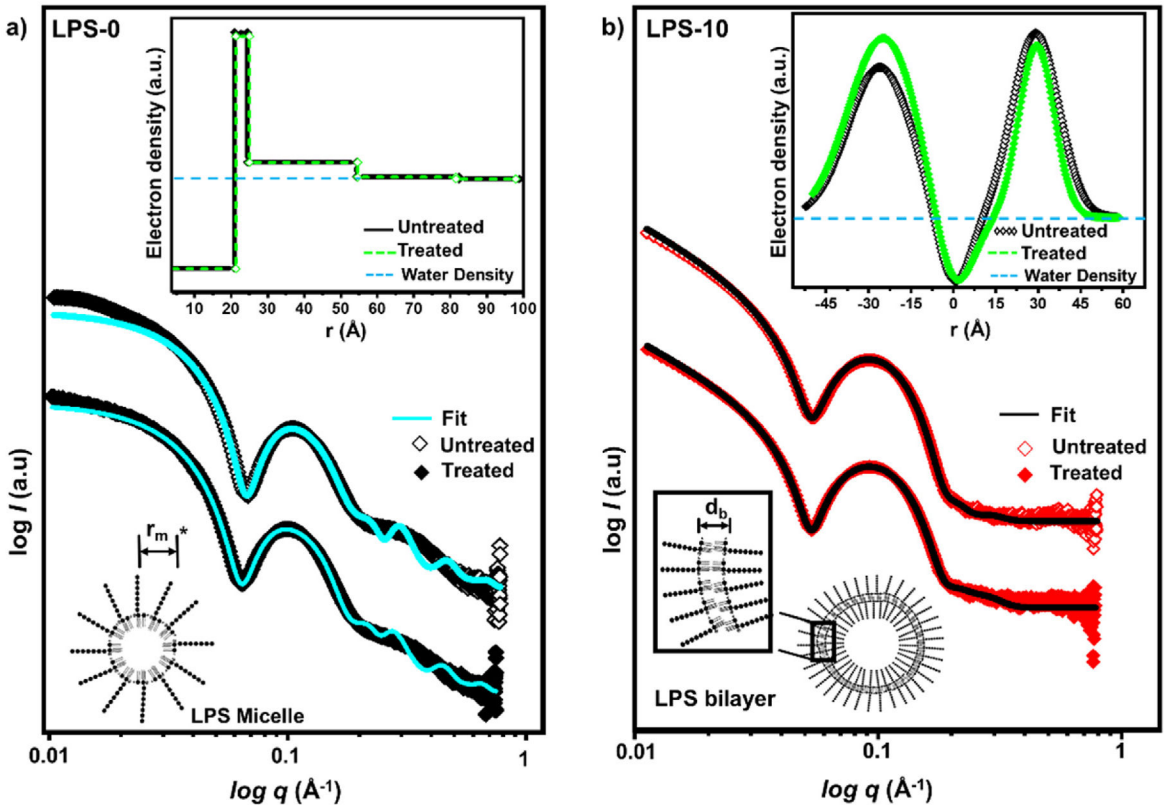

Fig. 3.

The patterns of small angle X-ray scattering (SAXS) for untreated and treated Ra lipopolysaccharide (LPS) (EH100) samples. Void and solid dot patterns represent data of untreated and treated LPS after hydrolysis, respectively. The curves of the untreated LPS samples have been vertically shifted for clarity. Scattering data and fit model for a) LPS-0 sample in pure water (black) and b) LPS-10 sample in presence of 10 mM $CaCl_2$ (red). Both graphs show insets of the structural electron density distributions. Illustrations of the represented distances shows the scattered electron density across the fitted model structures corresponding to the lipid moiety of the molecule. The marked asterisk (*) shown next to r_m in a) corresponds to the distance from the center to the second shell of the micellar fitted model. Please refer to the figure in supplementary information (Figure S1) for the distribution of the LPS-100 sample. (For interpretation of the references to color in this figure legend, the reader is referred to the Web version of this article.)

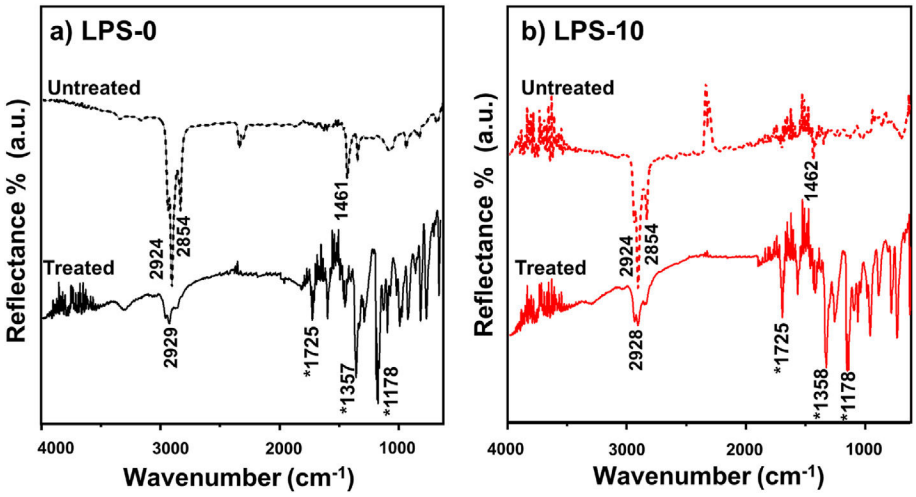

Fig. 4.

Fourier transform infrared (FTIR) spectra in grazing incidence reflectance mode of untreated and treated LPS (Ra EH100) samples. Spectra shown in a) LPS-0 and b) LPS-10. Asterisk (*) indicates the signals associated to the product of the hydrolysis.

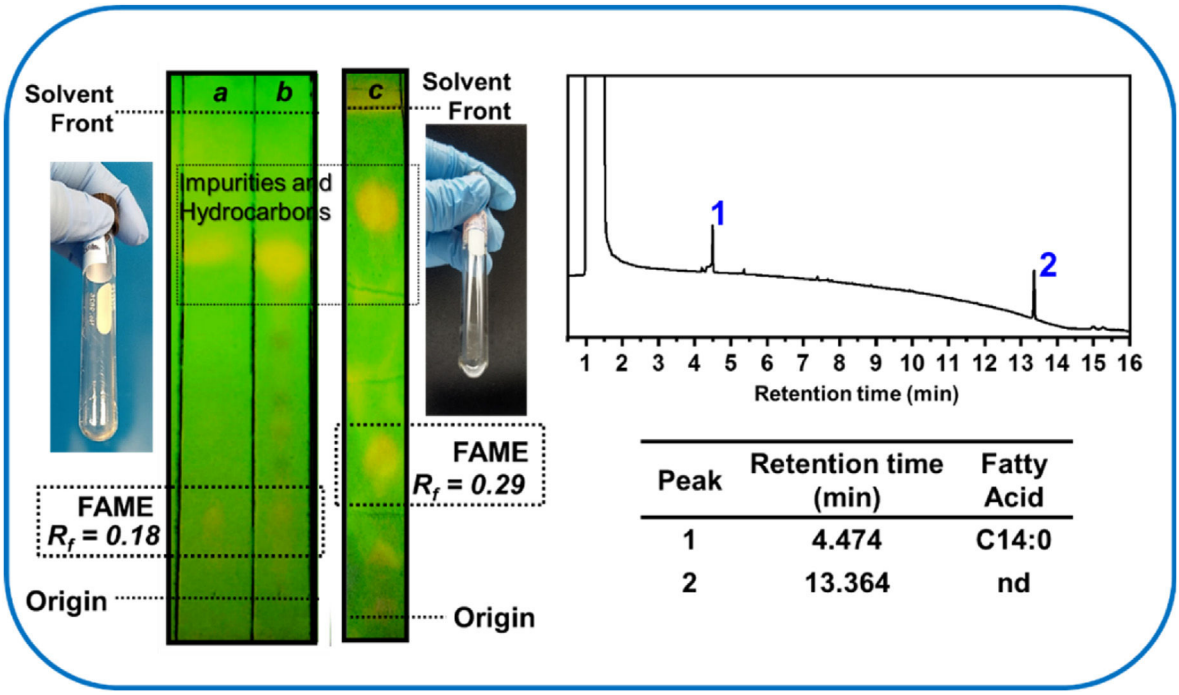

Peak	Retention time (min)	Fatty Acid
1	4.474	C14:0
2	13.364	nd

Fig. 5.

Images of fluorescent thin-layer chromatography (TLC plates (*far left*) showing separation of a) Fatty acid methyl ester (FAME) standard on the plate, FAME bands after the hydrolysis reaction in b) pure water, and c) in water with 10 mM Ca^{2+}. The insets illustrate product extraction after solvent removal for the hydrolysis reaction in pure water (left side over blue background) and water with 10 mM Ca^{2+} (right side over black background). Gas chromatography coupled with flame ionization detector (GC-FID) (*far right*) showing the presence of two FAME peaks corresponding to liberated free fatty acids after CALB hydrolysis. R_f, retention factor. (For interpretation of the references to color in this figure legend, the reader is referred to the Web version of this article.)

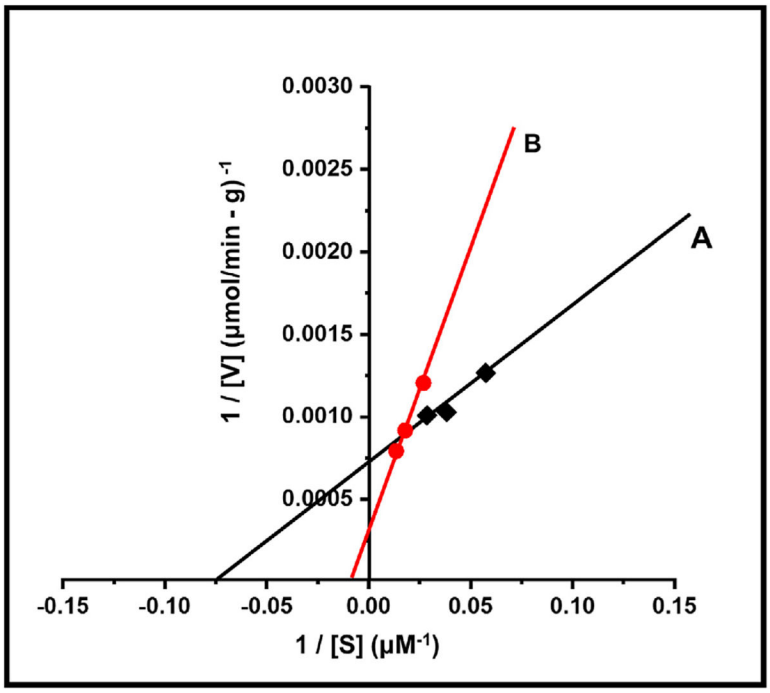

Fig. 6.

Lineweaver–Burk plot for FFA liberation using CALB and Ra LPS. Results show the liberated free fatty acid product for the hydrolysis conducted at 40 °C for the samples (A) LPS-0 and (B) LPS-10. V, velocity; S, substrate.

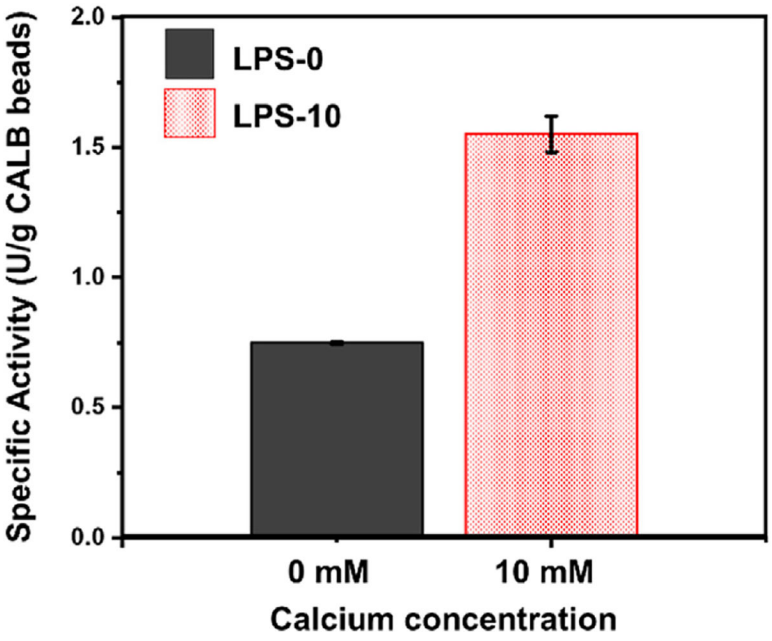

Fig. 7.

Specific activity (U/g CALB beads) showing liberated FFA after LPS hydrolysis in water (solid dark grey, LPS-0) and in water with 10 mM $CaCl_2$ (red pattern, LPS-10). Data denote the mean ± SD, n = 2. (For interpretation of the references to color in this figure legend, the reader is referred to the Web version of this article.)

Table 1

Summary of SAXS results structural data by the fit analysis.

	LPS-0		LPS-10	
	untreated	**treated**	**untreated**	**treated**
Structure	Micelle	Micelle	Bilayer	Bilayer
Size, [Å]	58.5 ± 4.0[a]	55.9 ± 4.0[a]	55.2 ± 1.1[b]	54.4 ± 1.1[b]
Width σ, *[Å]*	*na*	*na*	8.2 ± 0.1	6.2 ± 0.1

[a] corresponds to the r_m distance (illustration in Fig. 3a) from the center to the second shell of the micellar fitted model; and

[b] = results correspond to distance of the bilayer d_b (illustration in Fig. 3b).

The term *na* refers to not applicable.

Table 2

Kinetic parameters for CALB–Ra LPS system.

Sample	*Vmax (μmol/min*$^{-1}$ **per** *gm* $_{CALB\ beads}$*)*	*Km (μM)*
LPS-0	1.41×10^3	28.6
LPS-10	2.71×10^3	84.2